Journal of Alloys and Compounds 489 (2010) 252–256

Contents lists available at ScienceDirect

Journal of Alloys and Compounds

journal homepage: www.elsevier.com/locate/jallcom

Designed synthesis of wide range microwave absorption Fe_3O_4–carbon sphere composite

Shibing Ni, Xinghui Wang, Guo Zhou, Feng Yang, Junming Wang, Deyan He*

Department of Physics, Lanzhou University, Tianshui Road, Lanzhou 730000, China

ARTICLE INFO

Article history:
Received 26 June 2009
Received in revised form
12 September 2009
Accepted 14 September 2009
Available online 23 September 2009

Keywords:
Fe_3O_4–carbon sphere composite
Wide range microwave absorption

ABSTRACT

Fe_3O_4–carbon sphere composite was synthesized by a simple hydrothermal method. The as-synthesized products were characterized by field-emission scanning electron microscopy (FE-SEM), energy dispersive spectrum (EDS), X-ray diffraction (XRD), vibrating sample magnetometer (VSM), and Raman spectrum. The complex permittivity and permeability of paraffin wax and Fe_3O_4–carbon sphere composite with different volume fraction of the composite were measured by vector network analysis. A wide region of microwave absorption was achieved due to dual dielectric and magnetic losses. When the matching thickness is 4 mm, the calculated reflection loss of the sample with 70% volume fraction of Fe_3O_4–carbon sphere composite exhibits a broad microwave absorption ranging from 2.5 to 18 GHz.

1. Introduction

During the past few years, there has been a growing and widespread interest in microwave-absorbing materials due to their military and civil applications such as stealth defense system [1,2], microwave interference protection [3], and microwave darkroom [4]. In general, microwave absorption materials can be divided into two types: magnetic materials and dielectric materials, which are relevant to magnetic loss and dielectric loss, respectively. Recently, composite microwave absorption materials have attracted much attention due to their enhanced microwave absorption properties, which are relevant to multiform electromagnetic losses based on magnetic or dielectric loss [5–9,3]. We have reported hydrothermal synthesis of well dispersed Fe_3O_4 nanoparticles and their microwave absorption properties earlier. The as-prepared Fe_3O_4 nanoparticles exhibit excellent microwave absorption property, which is relevant to magnetic loss [10]. When the matching thickness is 3 mm, the calculated reflection loss reaches a maximum value of −21.2 dB at 8.16 GHz with 30% volume fraction of Fe_3O_4. In addition, graphitic carbon nanocoil was reported to be of outstanding microwave absorption properties owing to its dielectric loss [11]. Therefore, we are interested in designing Fe_3O_4–carbon composite material because their microwave absorption properties can be improved by dual magnetic and dielectric losses. Moreover, the reflection loss of Fe_3O_4 nanoparticles occurs at low frequency region below 10 GHz, while the reflection loss of carbon nanocoil occurs at high frequency region above 10 GHz, so dual magnetic and dielectric losses of the composite is hopeful to lead to broad range of microwave absorption. In this paper, the main objective is to design a wide range microwave absorption material through dual dielectric and magnetic losses. For such a purpose, Fe_3O_4–carbon sphere composite was synthesized by a simple hydrothermal method, and the dielectric and magnetic loss and microwave absorption properties were characterized and investigated by measuring the complex permittivity and permeability of the mixture of paraffin wax and Fe_3O_4–carbon composite and calculating.

2. Experimental details

Glucose and sodium sulfate were analytical grade and purchased from Shanghai Chemical Reagents, and Fe_3O_4 nanoparticles were prepared by a simple hydrothermal method [10]. In a typical procedure, 2 mmol glucose and 1 g sodium sulfate were dissolved in 60 ml distilled water. After stirring for 20 min, 1.39 g Fe_3O_4 nanoparticles was added in the solution and ultrasonically oscillated for 10 min. Then the black suspension was transferred into a 100 ml teflonlined autoclave, distilled water was subsequently added to 80% of its capacity. The autoclave was at last sealed and placed in an oven, heated at 160 °C for 24 h. After the reaction, the autoclave was cooled in air. The suspension was centrifuged sequentially with distilled water and ethanol both four times at 6000 rpm for 5 min. The resulting black precipitates finally were dried in an oven at 60 °C for 24 h.

The structures of the resulting products were characterized by X-ray powder diffraction (Rigaku RINT2400 with Cu Kα radiation) and Micro-Raman spectrometer (Jobin Yvon LabRAM HR800 UV, YGA 532 nm). Field-emission scanning electron microscopy (FE-SEM S-4800, Hitachi) equipped with energy dispersive spectrum (EDS) were employed for the morphology, size and composition analysis. For EDS characterization, the sample was dispersed in ethanol and dropped on Cu sheet. The magnetic properties of the products were characterized by vibrant sample magnetometer (VSM, Lakeshore 7304, USA). The compound samples were prepared by mixing the Fe_3O_4–carbon sphere and paraffin wax with Fe_3O_4–carbon sphere volume fraction ranging from 20% to 70%. The mixture was then pressed into toroidal shape with an outer diameter of 7 mm, inner diameter of 3.04 mm, and a thickness

* Corresponding author. Fax: +86 931 8913554.
E-mail address: hedy@lzu.edu.cn (D. He).

0925-8388/$ – see front matter © 2009 Elsevier B.V. All rights reserved.
doi:10.1016/j.jallcom.2009.09.065

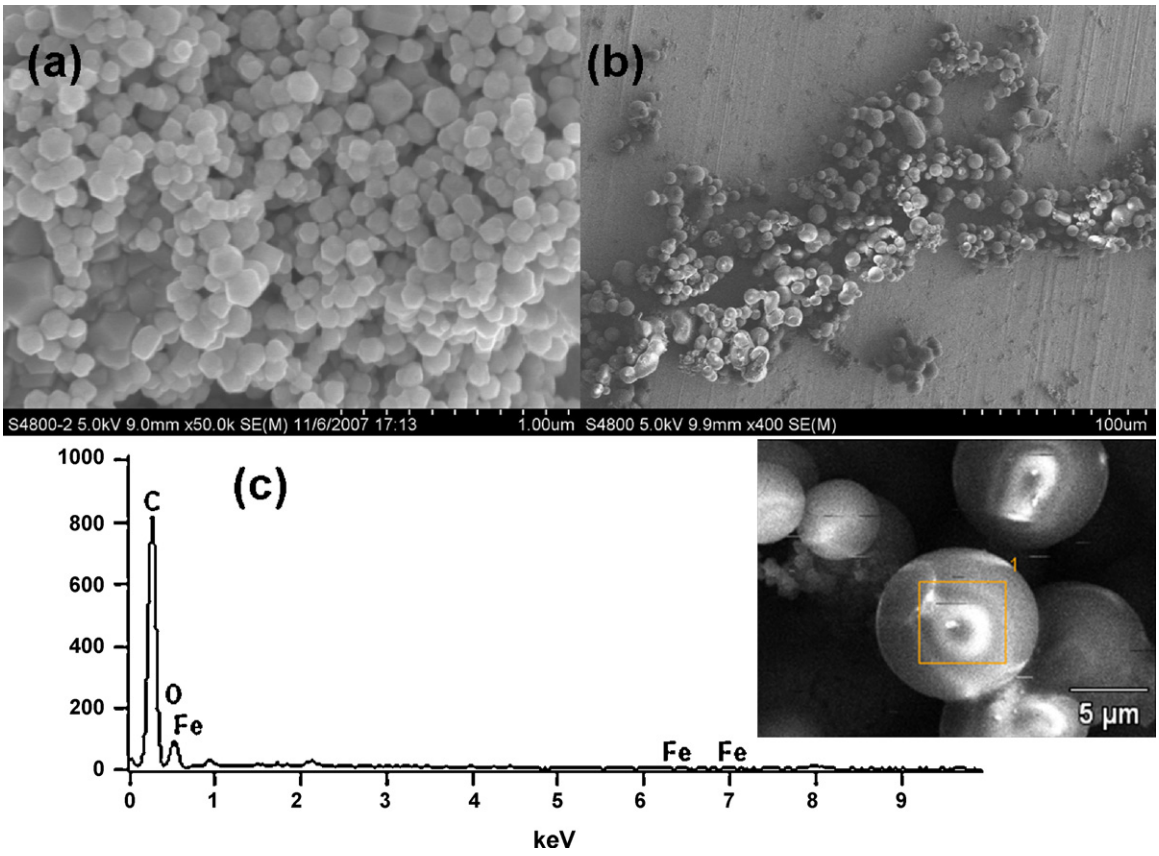

Fig. 1. SEM images of (a) Fe_3O_4 nanoparticles and (b) Fe_3O_4–carbon composite. (c) EDS image of Fe_3O_4–carbon composite; the corresponding SEM image was shown in insert in (c).

of 2 mm for microwave measurement. The complex permittivity and permeability of the compound samples were measured using an vector network analyzer (Agilent E8363B) in 0.1–18 GHz region and the reflection loss was calculated using the measured complex permittivity and permeability.

3. Results and discussion

Fig. 1a is the SEM image of Fe_3O_4 nanoparticles used in the synthesis of Fe_3O_4–carbon composite. General sphere like morphology is clearly revealed with mean diameter of about 150 nm. Fig. 1b shows a SEM image of the obtained Fe_3O_4–carbon composite. It is found that the mean diameter of those spheres is about 8 μm. The size of those spheres is much bigger than that of carbon spheres reported in literature [12], which may be affected by the agglomeration of magnetic Fe_3O_4. EDS characterization provides further information for the evaluation of the composition of the composite, which was shown in Fig. 1c. C, Fe, and O elements can be clearly identified from the EDS image. The signal near 1 keV attributes to Cu sheet. The insert in Fig. 1c shows the SEM image of the sphere where the EDS characterization was took place.

Fig. 2a presents the typical XRD pattern of the products. The peaks can be indexed as face centered cubic Fe_3O_4 with lattice constant a = 8.391 Å, which is in good agreement with JCPDS, No. 19-0629. The small peaks other than those from Fe_3O_4 may come from

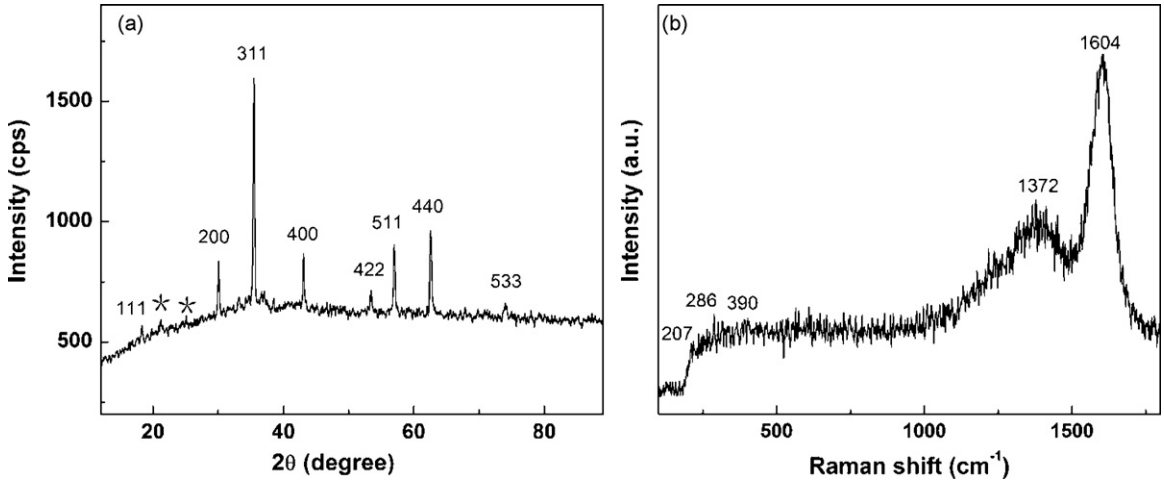

Fig. 2. XRD pattern (a) and Raman spectrum (b) of the products.

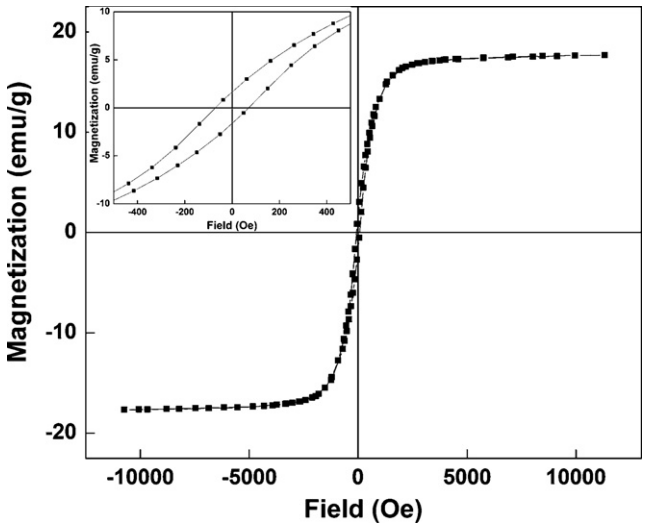

Fig. 3. Room-temperature magnetic hysteresis curve of the product; the insert is corresponding part hysteresis curves (field from −500 to 500 Oe).

carbon (marked with *) [13]. The oxidation of Fe_3O_4 was prevented due to the reductive property of glucose. The Raman spectrum of the composite was shown in Fig. 2b. In low wave number region, there are peaks at 207, 286, 390 cm^{-1}, which are in accordance with that of Fe_3O_4 [14]. In high wave number region, there are two peaks, one at 1372 cm^{-1} and the other at 1604 cm^{-1}. In Raman study, it is well known that the peak at 1580 cm^{-1} is characteristic of crystalline graphite (G-band), while the peak at 1350 cm^{-1} (D-band) is due to disorder of carbon materials [15]. It is apparent that the Fe_3O_4–carbon composite was composed of Fe_3O_4 and graphite with defects.

Fig. 3 shows the hysteresis loop of the as-synthesized Fe_3O_4–carbon composite. The saturation magnetization value was measured to be 17.6 emu/g, which is lower than that of pure Fe_3O_4 nanoparticles [10] (75.37 emu/g) due to the presence of carbon sphere. According to the saturation magnetization value of pure Fe_3O_4 nanoparticles and Fe_3O_4–carbon composite, it can be estimated that the mass percentage of Fe_3O_4 is about 23%. Furthermore, the insert part hysteresis curve reveals the coercivity of the products is 60.2 Oe, which is much lower than that of bulk Fe_3O_4 (115–150 Oe), and in accordance with that of Fe_3O_4 nanoparticles [10].

The complex permittivity of Fe_3O_4–carbon composite and paraffin wax composites with Fe_3O_4–carbon volume fraction ranging from 20% to 70% are presented in Fig. 4. It can be seen that the values of the complex dielectric constant do not significantly decrease with increasing frequency. For real part of complex permeability ε', the values show insignificant variation at frequency ranging from 0.1 to 18 GHz, which could be seen from Fig. 4a. For imaginary part of complex permeability ε'', it can be noticed from Fig. 4b that ε'' exhibit three resonance peaks. The first one lays near 1.75 GHz, the second one lays near 7.5 GHz, and the third one lays near 13.5 GHz. The resonance peaks were usually attributed to interfacial polarization [16], and we propose interfaces between Fe_3O_4 nanoparticles and carbon spheres and polarization in Fe_3O_4 nanoparticles are the causing of the resonance peaks. The polarization in ferrites has largely been attributed to the presence of Fe^{2+} ions which give rise to heterogeneous spinel structure. Since Fe^{2+} ions are easily polarisable, the larger the number of Fe^{2+} ions the higher would be the dielectric constant [17]. Furthermore, it can be noticed that the values of both ε'' and ε'' increase with volume concentration due to the enhancement of the interfacial polarization. The emergency of some intercross of ε' between 30% and 40% volume fraction may come from the errors of the measuring system.

Fig. 5 shows the complex permeability (real part Fig. 5a and imaginary part Fig. 5b) of the compound with Fe_3O_4–carbon volume fraction ranging from 20% to 70% in the frequency of 0.1–18 GHz. It is found that both the real part and imaginary part of permeability increase with composite volume fraction firstly and then decrease. For the real part of permeability μ', the values decrease along with the frequency, which was shown in Fig. 5a. Fig. 5b is frequency dependence imaginary part of permeability $\mu''$of the mixture. It shows three resonance peaks near 4.4, 10.2, and 15.1 GHz, respectively. The first peak comes from the natural resonance [18], whereas the resonance frequency is much bigger than that of pure Fe_3O_4 nanoparticles [10,19]. The other two peaks ascribe to exchange resonance, which is similar with that of spherical, monodispersed, ferromagnetic, metallic particles with equivalent size [19].

In order to investigate the intrinsic reasons for microwave absorption of Fe_3O_4–carbon composite, we calculated the dielectric and magnetic dissipation factor ($\tan\delta_E = \varepsilon'/\varepsilon''$, $\tan\delta_M = \mu'/\mu''$,). It can be seen from Fig. 6a that both the dielectric and magnetic loss do contribute to the microwave absorption. The total electromagnetic loss behavior is similar with that of magnetic loss, but with bigger value than that. Conventionally, the permittivity can generally be represented by Debye dipolar relaxation expression

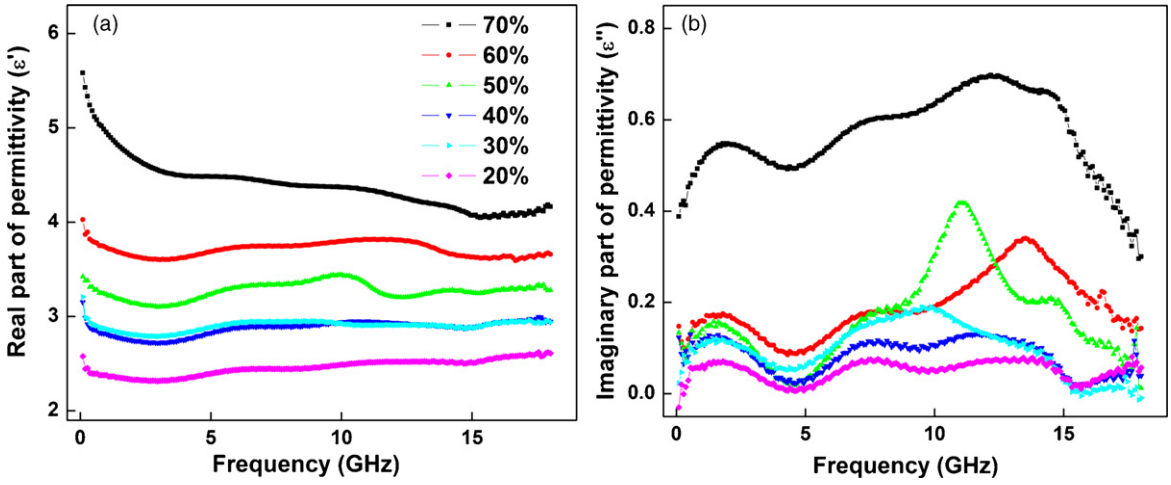

Fig. 4. Real part ε' (a) and imaginary part ε'' (b) of complex permittivity of the mixture of Fe_3O_4–carbon composite and paraffin wax with different volume fraction of composite.

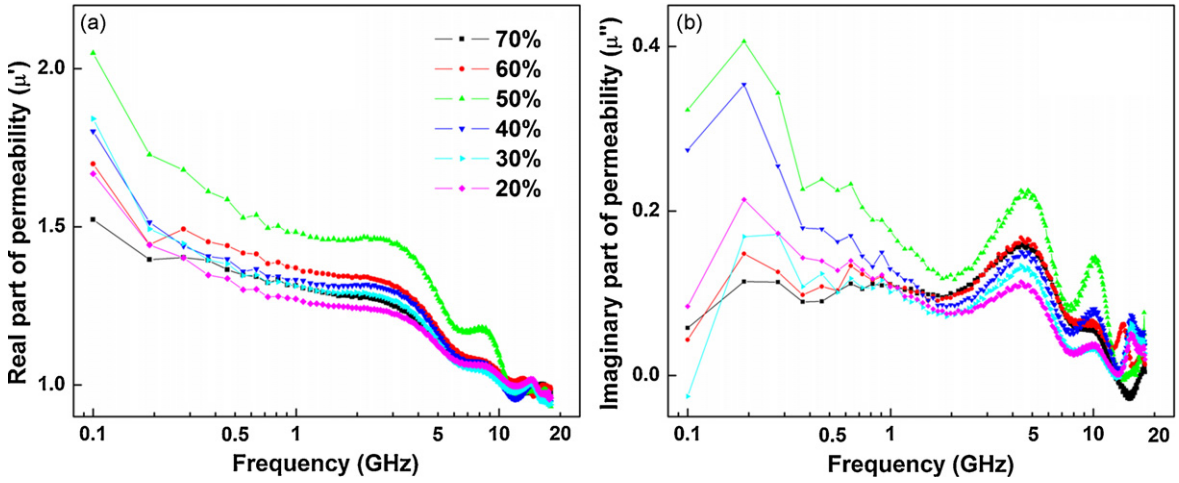

Fig. 5. Real part μ'(a) and imaginary part μ'' (b) of complex permeability of the mixture of Fe_3O_4–carbon and paraffin wax with different volume fraction of composite.

[20],

$$\varepsilon_r = \varepsilon_\infty + \frac{\varepsilon_s - \varepsilon_\infty}{1 + j2\pi f\tau} = \varepsilon'(f) + i\varepsilon''(f) \quad (1)$$

where f, τ, ε_s, and ε_∞ are the frequency, relaxation time, stationary dielectric constant, and optical dielectric constant, respectively. From Eq. (1), it can be deduced that,

$$\varepsilon'(f) = \varepsilon_\infty + \frac{\varepsilon_s - \varepsilon_\infty}{1 + (2\pi f)^2\tau^2} \quad (2)$$

$$\varepsilon''(f) = \frac{2\pi f\tau(\varepsilon_s - \varepsilon_\infty)}{1 + (2\pi f)^2\tau^2} \quad (3)$$

According to Eqs. (2) and (3), $(\varepsilon' - \varepsilon_\infty)^2 + (\varepsilon'')^2 = (\varepsilon_s - \varepsilon_\infty)^2$, and the plot of ε' versus ε'' should be a single circle, which was defined as Cole–Cole semicircle. Fig. 6b shows the curve characteristics of ε' versus ε'' for the sample with 70% volume fraction of Fe_3O_4–carbon composite. The presence of two semicircles suggests that there are dual dielectric relaxation processes. Interfaces between Fe_3O_4 nanoparticles and carbon sphere are the causing of dual dielectric losses.

The relation between the reflection of compound and the microwave frequency in the region of 0.1–18 GHz was shown in Fig. 7. It was calculated as follows:

$$Zin = \sqrt{\frac{\mu_r}{\varepsilon_r}}\tanh\left[j\frac{2\pi fd\sqrt{\mu_r\varepsilon_r}}{c}\right] \quad (4)$$

$$RL = 20Lg\left|\frac{Zin - 1}{Zin + 1}\right| \quad (5)$$

where μ_r and ε_r are the relative complex permeability and permittivity of the composite medium respectively, c is the speed of light, f is the frequency of microwaves and d is the thickness of the absorber. Fig. 7a is the calculated frequency dependence reflection loss of composite with Fe_3O_4 volume fraction ranging from 20% to 70% at the layer thickness of 4 mm. It can be noticed that the reflection loss peak shifts to low frequency along with increased Fe_3O_4–carbon composite volume fraction and the peak value becomes firstly bigger and then smaller. When the volume fraction is up to 70%, the reflection loss reaches a broadest band ranging from 2.5 to 18 GHz. For a contrast, thickness dependent reflection loss of the composite is also researched. Fig. 7b shows the calculated frequency dependence reflection loss of the sample with 70% Fe_3O_4–carbon composite volume fraction for layer thickness ranging from 2 to 7 mm. It is found that broad reflection losses were achieved and the peak value is enhanced with increasing thickness, shifting to lower frequency. Additionally, from the permittivity and permeability data shown in Figs. 4 and 5, it seems that both the dielectric loss and magnetic loss show distinct change.

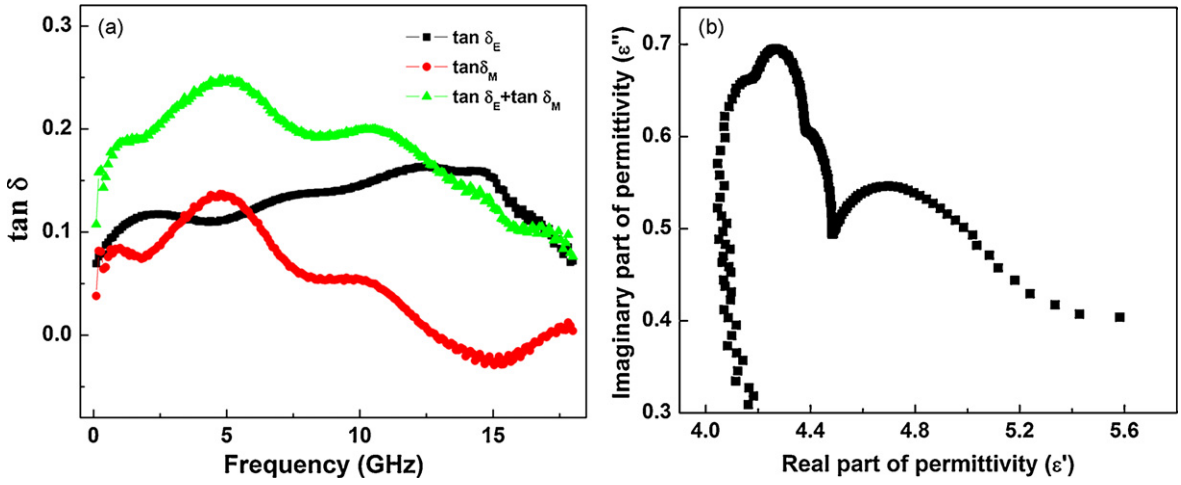

Fig. 6. Frequency dependence tan δ (a) (tan δ_E, tan δ_M, and tan δ_E + tan δ_M) and (b) typical Cole–Cole semicircle of the sample with 70% volume fraction of Fe_3O_4–carbon.

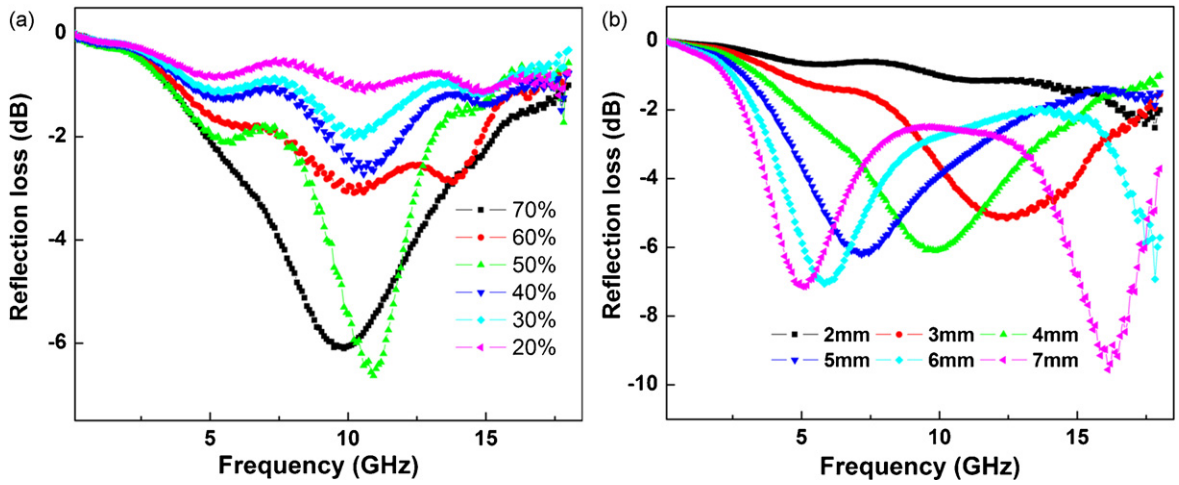

Fig. 7. Reflection loss of (a) composite with different volume fraction for layer thickness of 4 mm and (b) sample with 70% volume fraction of Fe_3O_4–carbon composite for different layer thickness.

Furthermore, according to expressions (4) and (5), it can be seen that the combinations of both μ_r and ε_r determine the reflection loss. Thus, the primary variation of reflection loss with frequency can be considered to be the integrated result of dielectric loss and magnetic loss [21].

4. Conclusions

In conclusion, broad microwave absorption ranging from 2.5 to 18 GHz was successfully achieved by designed synthesis of Fe_3O_4–carbon composite that are of dual dielectric and magnetic loss. The wide range microwave absorption properties makes it to have potential applications in microwave interference field. This study way will undoubtedly become a focus for the design and research of wide range microwave absorption material. However, the value of reflection loss peak is low, which may due to the unmatched size of Fe_3O_4 and carbon. Further work should be done on regulating the size of carbon sphere and Fe_3O_4 nanoparticles to reach an appropriate match of size and an optimum co-effect of dielectric and magnetic loss.

Acknowledgement

We gratefully acknowledge the financial support from the Teaching and Research Award Program for Outstanding Young Teachers in High Education Institutions of MOE, China.

References

[1] T. Giannakopoulou, L. Kompotiatis, A. Kontogeorgakos, G. Kordas, J. Magn. Magn. Mater. 246 (2002) 360–365.
[2] S.P. Ruan, B.K. Xu, H. Suo, F.Q. Wu, S.Q. Xiang, M.Y. Zhao, J. Magn. Magn. Mater. 212 (2000) 175–177.
[3] P. Saini, V. Choudhary, B.P. Singh, R.B. Mathur, S.K. Dhawan, Mater. Chem. Phys. 113 (2009) 919–926.
[4] BARTONDK, Radar Evaluation Handbook [M], Artech House, New York, 1998.
[5] G.Q. Wang, X.D. Chen, Y.P. Duan, S.H. Liu, J. Alloys Compd. 454 (2008) 340–346.
[6] X.A. Li, X.J. Han, Y.J. Tan, P. Xu, J. Alloys Compd. 464 (2008) 352–356.
[7] D.L. Zhao, Q. Lv, Z.M. Shen, J. Alloys Compd. 480 (2009) 634–638.
[8] F. Tabatabaie, M.H. Fathi, A. Saatchi, A. Ghasemi, J. Alloys Compd. 470 (2009) 332–335.
[9] S. Choopani, N. Keyhan, A. Ghasemi, A. Sharbati, R.S. Alam, Mater. Chem. Phys. 113 (2009) 717–720.
[10] S.B. Ni, S.M. Lin, Q.T. Pan, F. Yang, K. Huang, D.Y. He, J. Phys. D: Appl. Phys. 42 (2009) 055004 5.
[11] N.J. Tang, W. Zhong, C. Au, Y. Yang, M. Han, K. Lin, Y.W. Du, J. Phys. Chem. C 112 (2008) 19316–19323.
[12] X.M. Sun, Y.D. Li, Angew. Chem. Int. Ed. 43 (2004) 597–601.
[13] H. Liu, G.X. Wang, J.Z. Wang, D. Wexler, Electrochem. Commun. 10 (2008) 1879–1900.
[14] F.Y. Cao, C.L. Chen, Q. Wang, Q.W. Chen, Carbon 45 (2007) 727–731.
[15] G.Y. Zhang, X. Jiang, E.G. Wang, Appl. Phys. Lett. 84 (2004) 2646–2648.
[16] X.L. Dong, X.F. Zhang, H. Huang, F. Zuo, Appl. Phys. Lett. 92 (2008) 013127 3.
[17] H.J. Zhang, Z.C. Liu, C.L. Ma, X. Yao, L.Y. Zhang, M.Z. Wu, Mater. Sci. Eng. B 96 (2002) 289–295.
[18] C. Kittel, Phys. Rev. 73 (1948) 155–161.
[19] G. Viau, F. Fiévet-Vincent, F. Fiévet, P. Toneguzzo, F. Ravel, O. Acher, J. Appl. Phys. 81 (1997) 2749–2754.
[20] J. Frenkel, J. Dorfman, Nature (London) 126 (1930) 274–275.
[21] G. Li, G.G. Hu, H.D. Zhou, X.J. Fan, X.G. Li, Mater. Chem. Phys. 101 (2002) 101–104.